Direct Measurement of Microstructural Avalanches during the Martensitic Transition of Cobalt Using Coherent X-Ray Scattering

Christopher Sanborn, Karl F. Ludwig, Michael C. Rogers, and Mark Sutton

Phys. Rev. Lett. **107**, 015702 — Published 30 June 2011

DOI: 10.1103/PhysRevLett.107.015702

Direct Measurement of Microstructural Avalanches During the Martensitic Transition of Cobalt Using Coherent X-ray Scattering

Christopher Sanborn, Karl F. Ludwig
Department of Physics, Boston University, Boston, Massachusetts 02215, USA

Michael C. Rogers, Mark Sutton
Department of Physics, McGill University, Montreal, Quebec H3A 2T8, Canada

(Dated: May 23, 2011)

Heterogeneous microscale dynamics in the martensitic phase transition of cobalt is investigated with real-time x-ray scattering. During the isothermal transformation of the high-temperature face-centered cubic phase to the low-temperature hexagonal close-packed phase, the structure factor evolution suggests that the process can conceptually be viewed as an initial period of rapid local transformation followed by a slower period during which stacking changes lead to strain relaxation. Coherent x-ray scattering measurements show that, during the latter part of the transformation, the kinetics is dominated by discontinuous sudden changes – avalanches. The spatial size of observed avalanches varies widely, from 100 nm to the upper detection limit of 10 μm, which was the size of the x-ray beam. An empirical avalanche amplitude is defined to quantify the avalanche behavior; it exhibits a power-law size distribution. The avalanche rate decreases with inverse time since onset of the transformation.

PACS numbers: 61.05.cf, 81.30.Kf, 64.60.Ht, 64.60.av

It is becoming increasingly clear that the dynamics in many physical processes is fundamentally heterogeneous, as seen in such disparate systems as supercooled liquids [1], polymer melts [2], foams [3], granular flows [4], earthquakes [5, 6], ferromagnetic domain walls [7], and martensitic alloys [8–11]. A martensitic phase transition is a diffusionless structural transformation between two crystalline phases involving a rearrangement of atoms that shears the unit cell. This produces large coherency strains in the lattice as the new phase forms. As the transformation progresses, elastic energy accumulates and plays a major role in driving local dynamics. Measurements of transient thermal spikes [8, 9], acoustic emissions [9, 10], and electrical resistivity [11] during the athermal martensitic transition of multi-element alloys suggest they self-organize into a critical state that results in the relief of strain through a series of discrete avalanches. These measurement techniques, however, cannot probe structural details of the avalanches. Conventional x-ray and neutron scattering are standard tools for the investigation of evolving structure, but these measurements average incoherently over many regions of the sample and are therefore relatively insensitive to localized events. Coherent x-ray scattering at third-generation synchrotron sources, however, provides the means to overcome this limitation, using x-ray photon correlation spectroscopy (XPCS) to give direct access to the underlying local dynamics [12, 13]. This unique capability is used here to examine the heterogeneous evolution of local structure in cobalt as it undergoes a temperature-driven martensitic transformation.

Cobalt exhibits a martensitic phase transition between two close-packed structures, providing an interesting single-element system for probing structural evolution. The high temperature phase of cobalt is face-centred cubic (FCC), and the low temperature phase is hexagonal close-packed (HCP) [14]. The close-packed planes of these phases differ only in stacking order and interplanar spacing. The phase transition temperature for this first-order structural transformation is ~ 720 K, however this temperature migrates as the microstructure of cobalt evolves upon repeated cycling through the transition. This effect is most pronounced during the first ~ 20 transformation cycles [15].

Experiments reported here were performed on the 8-ID-E beamline at the Advanced Photon Source in Argonne National Laboratory. The beam was confined to a 10 μm $\times$ 10 μm area for the coherent experiments, and a 1340 $\times$ 1300 pixel deep depletion charged coupled device (CCD) was used to capture the scattered radiation. Images were collected from the CCD detector at a rate of 1.7 sec/frame. The CCD has a pixel size of 20 μm^2 and was placed 1.35 m from the sample. From these dimensions, the size of a single speckle on the detector is slightly larger than a single pixel. In addition to coherent experiments, "incoherent" experiments for sample characterization were performed with a 250 μm $\times$ 250 μm beam and a scintillation detector. A single crystal of cobalt that was previously cycled through the transition multiple times (~ 50) was used for all of the experiments reported here.

X-ray measurements on the cobalt sample were performed inside a custom-built chamber, with a base pressure of 10^{-6} torr to prevent oxidation of the sample at high temperatures. A hemispherical beryllium dome enabled access to a large range of scattering angles and enabled real-time scanning of the $(01.\mathrm{L})_{\mathrm{HCP}}$ and the $(00.\mathrm{L})_{\mathrm{HCP}}$ rods.

Prior to each experimental run the sample was typically annealed at 870 K until the FCC peak stopped evolving and no sign of the low-temperature HCP phase remained. The transition temperature T_{tr} for the sample was defined as the temperature at which the HCP phase was first observed during a slow cooling process. For each kinetics run, the sample was quenched at a rate of approximately 1 K/s from the anneal temperature to a final temperature $T < T_{tr}$. We define the effective quench temperature as $T_q = T_{tr} - T$. Upon quench completion, data collection continued in an isothermal setting.

The stacking order for the close-packed planes in the HCP phase is in the $[00.L]_{HCP}$ direction, resulting in a Bragg peak at $(00.2)_{HCP}$. In the same direction, the FCC close-packed planes result in a $(111)_{FCC}$ Bragg peak. There is a small difference between the inter-layer lattice spacing in the HCP and FCC phases, and this separates the location of their peaks. Both peaks were monitored throughout the transformation, as shown in the incoherent scattering pattern of Fig. 1a, where the two distinct peaks seen during the transformation process show that the transforming crystal is heterogeneous with two coexisting phases. For quenches near the transition temperature, remnants of the FCC phase persisted for the entire duration of the experiment (up to 8 hrs).

Evolution of the $(00.2)_{HCP}$ and $(111)_{FCC}$ Bragg peak integrated intensities, positions, and widths obtained from incoherent scattering patterns during the FCC-HCP transformation are shown in Fig. 1b-d, respectively. These values were extracted from Lorentzian fits of the data for each peak, as shown in Fig. 1a.

The two main factors that affect the Bragg peak width are the inhomogeneous strain and the size of coherently scattering regions, i.e. the domain size. Following the growth regime, the integrated intensity of each of the peaks remained roughly constant. However, the FCC peak broadened rapidly until it reached roughly the same width as the HCP peak. At this point, the rate of change in peak widths became significantly slower. This behavior suggests that the peak widths are primarily determined by inhomogeneous strains that have a similar size throughout the two phases. Thus, the evolution of the peaks suggest that the transformation occurs conceptually through two processes: an initial growth of the new HCP phase, followed by a strain redistribution through elimination of stacking faults. Local structural evolution during the formation of the HCP phase following a quench is relatively rapid; the focus of our coherent scattering studies discussed in the remainder of this paper is on characterizing discrete events in the evolution during the latter phase of the transformation.

A "waterfall" plot of typical x-ray speckle intensity evolution observed by coherent x-ray scattering near the $(00.2)_{HCP}$ peak during the latter part of the transformation is shown in Fig. 2 – it clearly shows the existence of sudden discontinuities in structural evolution,

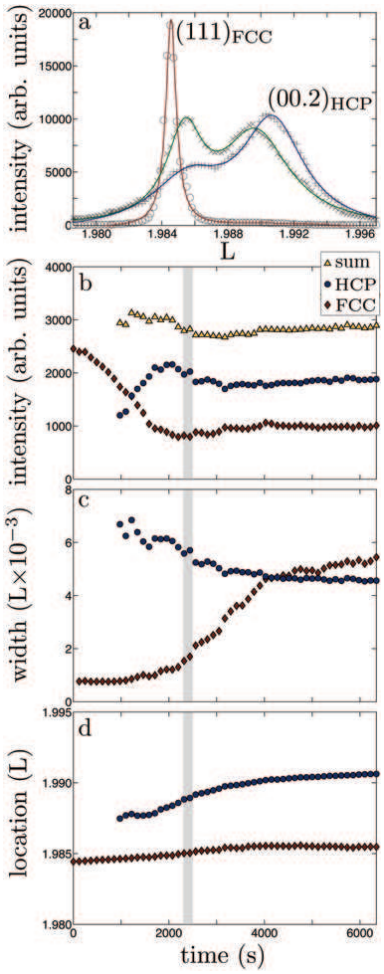

FIG. 1: (color online) a) The $(00.2)_{HCP}$ and $(111)_{FCC}$ Bragg peaks for three times during the FCC-HCP transformation during a quench to $T_q = -10$ K. The ∘ symbols represent data immediately following the quench (scaled down to 25% of their original value), × and + symbols represent data collected starting 3050 and 6344 seconds following quench onset, respectively. From Lorentzian fits of the data (shown as solid curves), the complete evolution of b) integrated intensity, c) width at half maximum, and d) location for both Bragg peaks were determined. The integrated intensity sum from both Bragg peaks is also shown in b). Growth and strain redistribution stages of the transition are separated by the vertical grey lines in b)-d).

i.e. avalanches. In this figure a large avalanche is seen at approximately 10 minutes, however the majority of avalanches observed were more comparable to the small avalanche seen at approximately 7 minutes. Most avalanches affected a well-defined region in reciprocal space no larger than 20-30 speckles. This corresponds to spatial extents up to several hundred nanometers. Some avalanches were confined to regions as small as a single speckle, however, suggesting a change across the entire illuminated sample volume. Avalanches occur during the

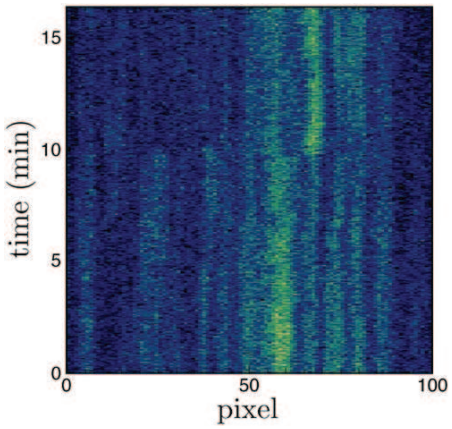

FIG. 2: (Color online) A "waterfall" plot showing the evolution of a 100 pixel cross section of a speckle pattern near the $(00.2)_{\mathrm{HCP}}$ peak during a phase transformation. Abrupt changes in pixel intensity such as the one at approximately 10 minutes indicate the occurrence of avalanches. A smaller avalanche occurs at approximately 7 minutes.

second phase of the transition, when the volume fraction of each phase remains relatively constant, implying that avalanche activity involves rearrangement of domains in both phases.

XPCS studies of nonequilibrium systems have often used two-time corrrelation functions to analyze the system dynamics [13]. Homogeneous dynamics results in a Gaussian distribution of two-time correlation values [16]. A characteristic of heterogeneous dynamics is deviation from this distribution, which we have determined to be the case for the martensitic transition of cobalt. Identification of the individual avalanches indicative of the heterogeneous nature of this system requires going beyond standard two-time correlation analysis. The process used here to quantify avalanche evolution involved selecting 100×100 pixel areas in a region which had at least one photon per pixel per frame. These images were further subdivided into 10×10 bins, and from each bin n two-time difference values were calculated using

$$D_n(q, t_1, t_2) = \langle |I_n(q, t_1) - I_n(q, t_2)| \rangle \tag{1}$$

where $I(q,t)$ is the intensity and the average is over the 100 pixels in the bin. Figure 3a shows a representative example of two-time differences from a single bin for a quench below T_{tr}. The block-like structure of $D_n(q, t_1, t_2)$ reflects the heterogeneous nature of the dynamics. To quantify avalanche sizes and to improve statistics, we calculate two averages over the difference between two successive rows of D_n near the diagonal. These averages are

$$A_{n-}(q, t_1) = \frac{1}{m} \sum_{t_i = t_1 - m}^{t_1 - 1} [D_n(q, t_1, t_i) - D_n(q, t_1 - 1, t_i)], \tag{2}$$

and

$$A_{n+}(q, t_1) = \frac{1}{m} \sum_{t_i = t_1 + 1}^{t_1 + m} [D_n(q, t_1 - 1, t_i) - D_n(q, t_1, t_i)], \tag{3}$$

where m is the number of time steps chosen for averaging. The change in the speckle pattern before and after t_1 is averaged to give the amplitude

$$A(\mathbf{q}, t_1) = (A_{n-} + A_{n+})/2. \tag{4}$$

For the data presented here, averages with $m = 15$ timesteps were chosen. No significant change in the results was found when changing this value.

To facilitate reliable detection of small avalanches we compare fluctuations from a given set of pixels to the fluctuations expected from photon statistics and detector noise. To characterize the noise distribution, the speckle pattern for a static sample of a disordered Fe_3Al crystal was measured. Our analysis normalizes the binned $A(\mathbf{q}, t_1)$ values by the equivalent values expected from the measured "static" noise. Using these values, a total "avalanche amplitude" $A(\sigma)$ is calculated by integrating the amplitudes above three standard deviations from the noise value. Figure 3b plots this total amplitude in units of standard deviations σ. Using this method, avalanches show up as distinct peaks in the amplitude, with peak values reflecting the amount of discontinuous change in the scattering pattern from each avalanche event.

The cumulative total of observed avalanches over time $N(t)$ following a quench at $t = 0$ is displayed in Fig. 3c. All avalanches were detected in isothermal conditions, revealing that thermal fluctuations play a significant role in the transition kinetics. At each T_q, $N(t)$ grew logarithmically in time: $N(t) = a\log(t) + C$, giving an avalanche rate that decreases with time as $dN/dt = a/t$. During the window of time that our observations were made, there was no evidence that avalanche amplitude depended on avalanche rate. The fit parameter a decreased for deeper quenches below T_{tr}, implying that thermal fluctuations at these lower temperatures were less likely to initiate avalanches. For quenches to room temperature, where $T_q \sim -400$ K, avalanches were not observed. Instead, two-time correlations between speckle patterns were similar to those observed in a homogeneous order-disorder phase transition [17], suggesting that averaging over many fluctuations in the domain walls was taking place. Previous studies used constant temperature ramping to produce avalanches in martensitic alloys [9–11], indicating that the energy barriers for their structural phase transitions are too large for thermal fluctuations to induce avalanches.

Avalanche amplitudes have a power-law distribution $N(A) \propto A^{-\alpha}$ with exponent $\alpha = 1.7 \pm 0.2$, as shown in Fig. 3d, exhibiting the absence of characteristic spatial scales in the underlying dynamics. Power-law distributions with varying exponents have previously been

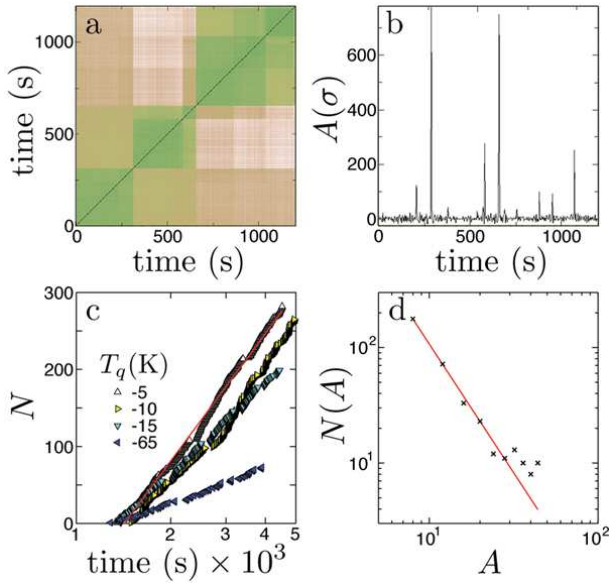

FIG. 3: (Color online) a) The two-time difference values for a quench to $T_q = -5$ K. b) Avalanche amplitudes calculated from the data in a). c) The cumulative number of avalanches over time $N(t)$ near the $(01.3)_{\mathrm{HCP}}$ peak for various T_q. The line is a fit of the logarithmic function to the $T_q = -5$ K data. d) A typical distribution of avalanche amplitudes during a phase transformation with a power-law fit of the data.

reported in the amplitude of thermal [8, 9] and acoustic [9, 10] measurements of avalanche activity during the martensitic transition in copper-based alloys, and also in electrical resistivity measurements in NiTi [11]. The effect of repeated cycling through the phase transformation has been shown to reduce the number of large avalanches in Cu-Zn-Al [8]. Such hysteresis effects are beyond the scope of this work, however the evolution of the microstructure and its contribution to these effects are accessible using speckle analysis, thus providing a clear direction for future work.

Interestingly, avalanche behavior during the isothermal martensitic transformation of cobalt shows significant similarities to earthquake statistics. The empirical laws found for earthquakes: the Gutenberg-Richter law [5] for their power-law magnitude distribution, and the Omori law [6] for the $1/t$ decrease in aftershock rate following the main earthquake, are analogous to the results obtained here. Aftershocks arise from the sudden relaxation of strain formed as the Earth's crust adjusts to a shift in the fault plane from the main shock. In the analogous situation with cobalt, coherency strains built up by the initial transformation of FCC to partially ordered HCP lattices are released through the sudden microstructural rearrangements observed in the avalanches. Despite the vastly different scales involved with microstructural avalanches and geological earthquakes, the behavioral characteristics they have in common suggests a remarkable similarity in their strain-relief dynamics.

In conclusion, we have used coherent x-ray scattering to develop the first direct structural probe of microstructural avalanches. Compared to most multi-element martensites studied, one expects that cobalt, involving only a single element and a transformation between the two close-packed structures fcc and hcp, will provide a straight forward model system in which to study thermally-driven martensitic phase transitions. In particular, the well-defined twinning boundaries in cobalt should lead to correlation in the speckle pattern, providing new avenues to gain insight into important issues such as the role that crystal defects play in hysteresis, and the nature of the heterogeneous dynamics.

We acknowledge helpful conversations about earthquake dynamics with William Klein and Christopher Serino (Boston University) and invaluable help from the staff at sector 8-ID who keep the beamline in excellent working order. The Boston University component of this research was supported by NSF DMR-0508630 (experiment) and U.S. DOE Office of Science, Office of Basic Energy Sciences DE-FG02-03ER46037 (development of algorithms for analysis of x-ray data from nonequilibrium systems). Use of the Advanced Photon Source was supported by the U.S. Department of Energy, Office of Science, Office of Basic Energy Sciences, under Contract No. DE-AC02-06CH11357.

[1] M. D. Ediger, Annu. Rev. Phys. Chem., **51**, 99 (2000).
[2] H. Guo *et al.*, Phys. Rev. Lett., **102**, 075702 (2009).
[3] M. M. Folkerts, S. W. Stanwyck, and O. G. Shpyrko *in preparation.*
[4] A. Abate and D. Durian, Chaos **17**, 041107 (2007).
[5] B. Gutenberg and C. F. Richter, Bull. Seismol. Soc. Am. **34**, 185 (1944).
[6] F. Omori, J. Coll. Sci. Imper. Univ. Tokyo **7**, 111 (1895).
[7] P. Cizeau, S. Zapperi, G. Durin, and H. E. Stanley, Phys. Rev. Lett. **79** 4669 (1997); D. H. Kim, S. B. Choe, and S. C. Shin, Phys. Rev. Lett. **90** 087203 (2003).
[8] L. Carrillo and J. Ortín, Phys. Rev. B, **56**, 11508 (1997).
[9] M. C. Gallardo, J. Manchado, F. J. Romero, J. del Cerro, E. K. H. Salje, A. Planes, and E. Vives, R. Romero, and M. Stipcich, Phys. Rev. B, **81**, 174102 (2010), and references therein.
[10] F. J. Pérez-Reche, E. Vives, L. Mañosa, and A. Planes, Phys. Rev. Lett., **87**, 195701 (2001).
[11] U. Chandni, A. Ghosh, H. S. Vijaya, and S. Mohan, Phys. Rev. Lett., **102**, 025701 (2009).
[12] M. Sutton *et al.*, Nature, **352**, 608 (1991).
[13] M. Sutton, C. R. Physique, **9**, 657 (2008).
[14] Co is ferromagnetic at this transition, but magnetism appears to play little or no role in this transition.
[15] A. Munier, J. E. Bidaux, R. Schaller, and C. Esnouf, J. Mater. Res., **5**, 769, (1990).
[16] A. Duri, H. Bissig, V. Trappe, and L. Cipelletti, Phys. Rev. E, **72**, 051401 (2005).
[17] A. Fluerasu, M. Sutton, and E. M. Dufresne, Phys. Rev.

Lett., **94**, 055501 (2005).

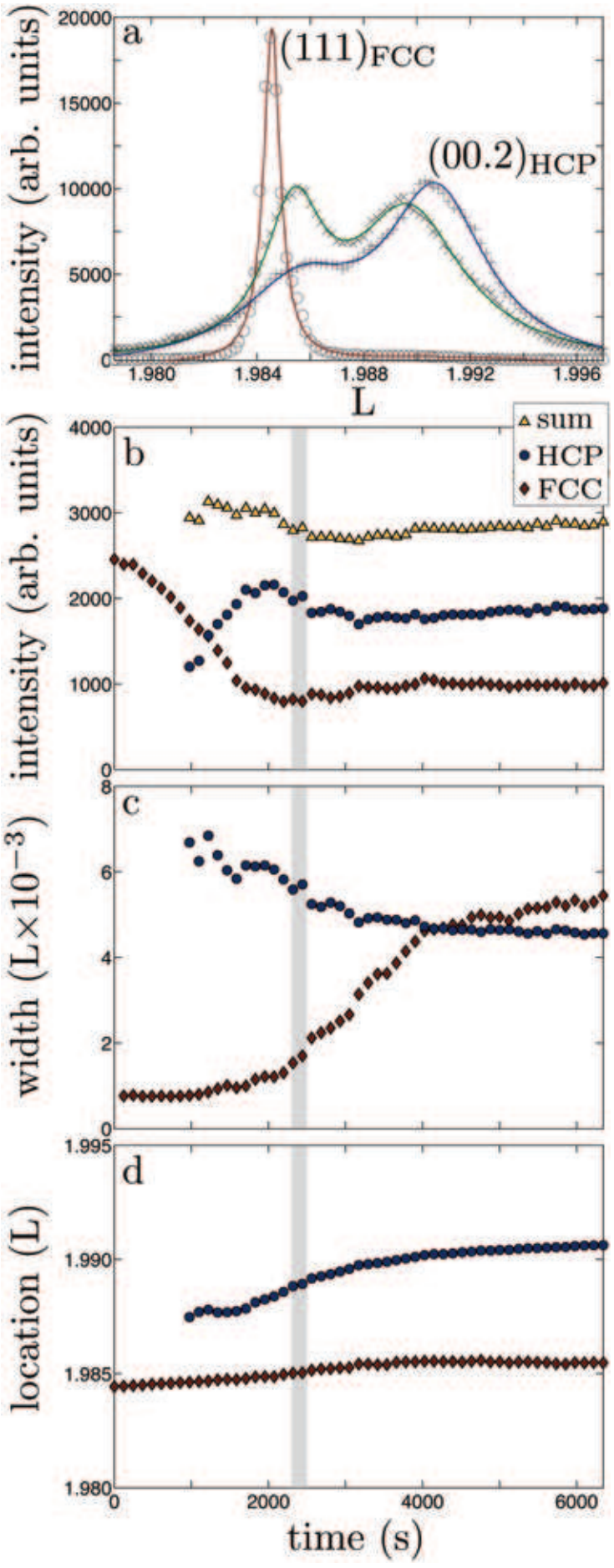

Figure 1 LD12997 23May2011

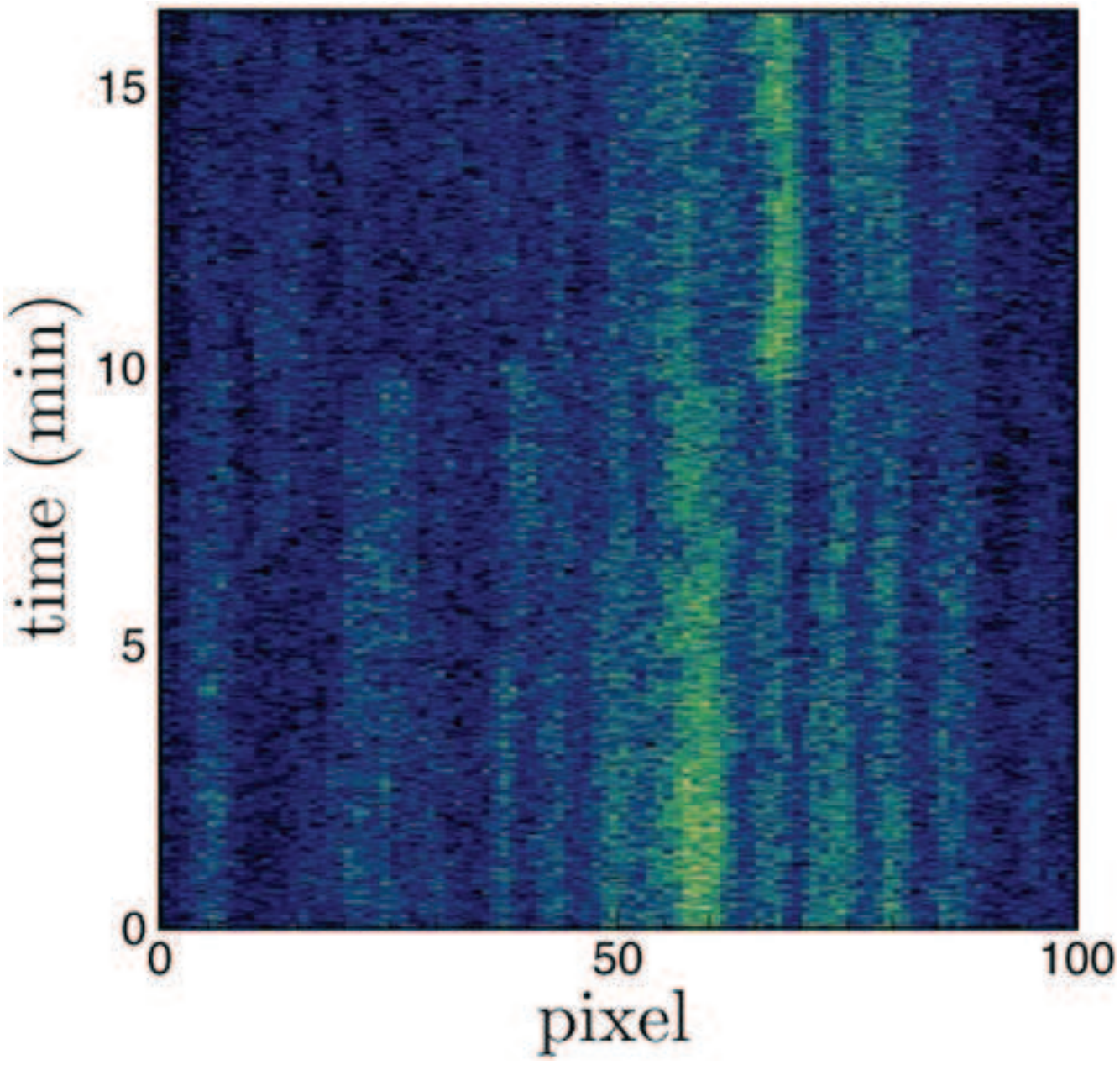

Figure 2 LD12997 23May2011

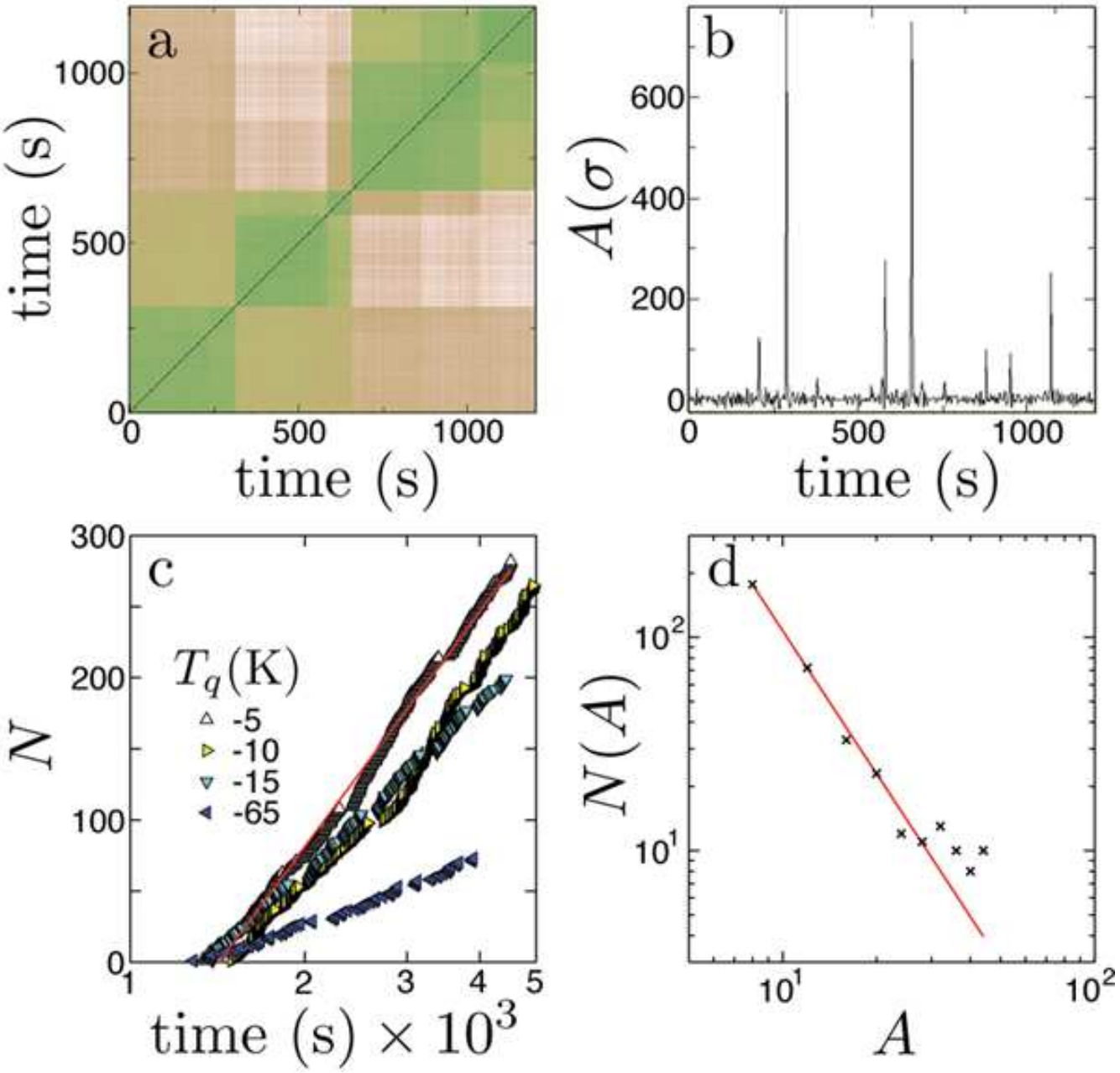

Figure 3 LD12997 23May2011